Vietnam Journal of Earth Sciences, 47(1), 118–135, https://doi.org/10.15625/2615-9783/22189

Vietnam Journal of Earth Sciences
https://vjs.ac.vn/index.php/jse

Enhancing spatial prediction of flash floods with Balancing Composite Motion Optimized Random Forest: A case study in High-Frequency Torrential rainfall area

Pham Viet Hoa[1], Nguyen An Binh[1], Pham Viet Hong[2], Nguyen Ngoc An[1], Giang Thi Phuong Thao[1], Nguyen Cao Hanh[1], Dieu Tien Bui[3,*]

[1]*Ho Chi Minh City Institute of Resources Geography, Vietnam Academy of Science and Technology, Mac Dinh Chi 1, Ben Nghe, 1 District, Ho Chi Minh City 700000, Vietnam*
[2]*Institute of Marine Geology and Geophysics, Vietnam Academy of Science and Technology, 18 Hoang Quoc Viet, Cau Giay District, Hanoi 10000, Vietnam*
[3]*GIS Group, Department of Business and IT, University of South-Eastern Norway, Gullbringvegen 36, 3800 Bø i Telemark, Norway*

Received 11 June 2024; Received in revised form 16 August 2024; Accepted 16 November 2024

ABSTRACT

Flash floods continue to emerge as a serious and growing natural hazard for many communities worldwide, especially in areas affected by tropical storms. These floods damage critical infrastructure and severely strain economic resources, underscoring the urgent need for advanced flood prediction tools. This study presents an innovative integrated machine learning approach, BCMO-RF, which merges Balancing Composite Motion Optimization (BCMO) with Random Forest (RF) to map flash flood susceptibility. In the BCMO-RF approach, the RF algorithm is applied to develop the flash flood model, while BCMO is used to explore and optimize the model's parameters. The study concentrates on areas in Thanh Hoa Province, Vietnam, frequently impacted by flash floods. Accordingly, various geospatial data sources were utilized to compile a geodatabase comprising 2,540 flash flood locations and 12 influencing factors. The geodatabase served as the basis for training and validating the BCMO-RF model. Results show that the BCMO-RF model attained high prediction accuracy (93.7%), achieving a Kappa coefficient of 0.874 and an AUC score of 0.988, outperforming the Deep Learning model benchmark. The study finds that the BCMO-RF model is reliable for accurately mapping areas susceptible to flash floods.

Keywords: Flash flood susceptibility, Random Forest; Balancing Composite Motion Optimization, GIS, Tropical areas.

1. Introduction

According to the Global Climate Risk Index 2020, Vietnam was ranked the sixth most affected country globally by climate variability and extreme weather events (Tuyet Hanh et al., 2020). The nation frequently experiences severe weather events, including typhoons, floods, droughts, and landslides, threatening its environment, economy, and communities (Group and Bank, 2021). Accordingly, floods constitute Vietnam's most significant economic risk, responsible for approximately 97% of the average annual losses from natural hazards. Projections

*Corresponding author, Email: Dieu.T.Bui@usn.no

indicate that due to climate change, the population affected by floods could increase by 3 to 10 million by 2035–2044 (Willner et al., 2018). Thus, investing in research and innovation is crucial to enhancing flood prediction methods and creating effective flood management strategies.

Floods in Vietnam can essentially be classified into river floods, coastal floods, urban floods, dam break floods, and flash floods. River flooding occurs when prolonged and heavy rainfall causes rivers to exceed their capacity, overflowing water into surrounding areas (Plate, 2007). This phenomenon develops gradually and can persist for several days, significantly inundating adjacent lands. Meanwhile, coastal floods occur when seawater inundates coastal areas, typically caused by storm surges, high tides, rising sea levels, or tsunamis, leading to potential damage and safety risks (Wdowinski et al., 2016). This rise is predominantly caused by tropical depressions or storms and strong winds, which drive water inland, resulting in flooding along the coast. Urban flooding occurs when excessive rainfall overwhelms the drainage system in densely populated areas, leading to the overflow of sewer pipes (Guo et al., 2021). This situation is exacerbated by continuous rainfall on impervious surfaces, which reduces the land's ability to absorb water, further contributing to the inundation. Dam break floods occur when flood protection structures fail as a result of extreme flood events (Wang et al., 2024). In contrast, flash flooding is a sudden surge of water in a stream or low-lying urban area, typically happening within six hours after a major rainfall event (Knocke and Kolivras, 2007).

Flash flooding is the most destructive and challenging to predict among these types of floods due to its rapid and sudden onset, strong flow velocities, and nonlinear dynamics (Wu et al., 2019), making it particularly hazardous. Literature review shows that spatial prediction of flash floods has seen significant advancements in the last ten years through hydrological models, geographic information systems (GIS), remote sensing, and machine learning techniques. Advanced hydrological models, such as Soil and Water Assessment Tool (SWAT) (Jodar-Abellan et al., 2019), the Hydrologic Engineering Center's Hydrologic Modeling System (HEC-HMS) (Sabău et al., 2023), and TELEMAC (Godara et al., 2023) have been employed to simulate flash flood scenarios. These models utilize a range of numerical formulas, from simple empirical equations to sophisticated differential formulations, to quantify rainfall-runoff dynamics. By considering factors such as precipitation, soil type, and land cover, they predict the spatial distribution of floodwaters. Generally, models are crucial for precisely forecasting flash floods across different spatial and time dimensions (Bournas and Baltas, 2022); however, they still depend on extensive long-term monitoring data for reliable predictions.

Recent developments in GIS, remote sensing technologies, and artificial intelligence have significantly advanced research in flash flood modeling and prediction (Amiri et al., 2024). Herein, satellite-based remote sensing provides real-time data crucial for monitoring and predicting flash flood events (Suresh et al., 2024). In contrast, GIS allows combining and examining multiple data layers, such as topography, land use, soil moisture, and rainfall intensity, for mapping flood-prone areas and identifying potential flash flood zones (Trong et al., 2023). While artificial intelligence, utilizing various advanced machine learning and deep learning techniques, can effectively predict flash flood-prone areas by leveraging historical flash flood records and multi-sourced geospatial data, i.e., extreme learning (Bui et al., 2019),

decision trees (Ngo et al., 2021), random forest (Abedi et al., 2022), long short-term memory (Zhao et al., 2022), and deep learning (Tsangaratos et al., 2023).

Recent research emphasizes the importance of integrating various predictive methods to enhance the reliability of flash flood prediction. The combination of GIS, remote sensing, and machine learning could provide a comprehensive approach to spatial prediction (Amiri et al., 2024). Despite advancements, predicting flash floods remains challenging due to the complex interactions between climatic, hydrological, and topographical factors. Thus, continued innovation and integration of these approaches are vital for improving the accuracy and reliability of flash flood forecasts, ultimately enhancing preparedness and resilience against these devastating events.

This study advances insights into flash flood modeling and prediction by introducing and validating a new integrated machine-learning approach named BCMO-RF. This approach integrates Balancing Composite Motion Optimization (BCMO) with Random Forest (RF) for flash flood susceptibility mapping, illustrated through a case study in a flood-prone region of Thanh Hoa Province, Vietnam. This methodology uses RF to develop the flash flood model while BCMO optimizes model parameters. The findings are subsequently assessed compared to cutting-edge ensemble learning and deep learning methods, followed by a summary of conclusions.

2. Study area and data used

2.1. Study area

Thanh Hoa Province (Fig. 1), located in Vietnam's north-central region, is selected as the study area for flash flood research due to its diverse topography, climatic conditions, and historical susceptibility to flash floods (Hoa et al., 2024). This makes it a valuable case for enhancing our understanding of flash flood dynamics and refining prediction techniques. Spanning approximately 11,080.8 square kilometers, the province features a varied landscape that includes mountainous regions, rivers, and coastal areas.

Thanh Hoa's topography is highly varied, ranging from the steep mountains of the western region to the flat, low-lying coastal plains in the east. This varied topography is considered a contributing factor to the region's complex flash flood dynamics. Additionally, the province is intersected by several major rivers, including the Ma and Chu rivers, significantly influencing the regional hydrological cycle. Besides, the province possesses an intricate system of rivers and streams (Linh et al., 2019) that can quickly swell during heavy rainfall, leading to sudden and severe flooding.

The climate of Thanh Hoa is tropical monsoon, with distinct wet and dry seasons (Dinh and Thi, 2024). The wet season in the province extends from May to October. It is characterized by substantial rainfall and a high frequency of storms, which often result in flash floods and landslides, particularly in the mountainous and hilly areas where rapid runoff can occur.

The province's economy relies heavily on agriculture, with a significant portion of the population residing in rural areas. These communities are often located in flood-prone zones, making them particularly susceptible to the impacts of flash floods. The combination of high population density in vulnerable areas and limited infrastructure for flood management heightens the need for effective flash flood prediction and mitigation strategies. More information about this study area can be found in Hoa et al. (2024).

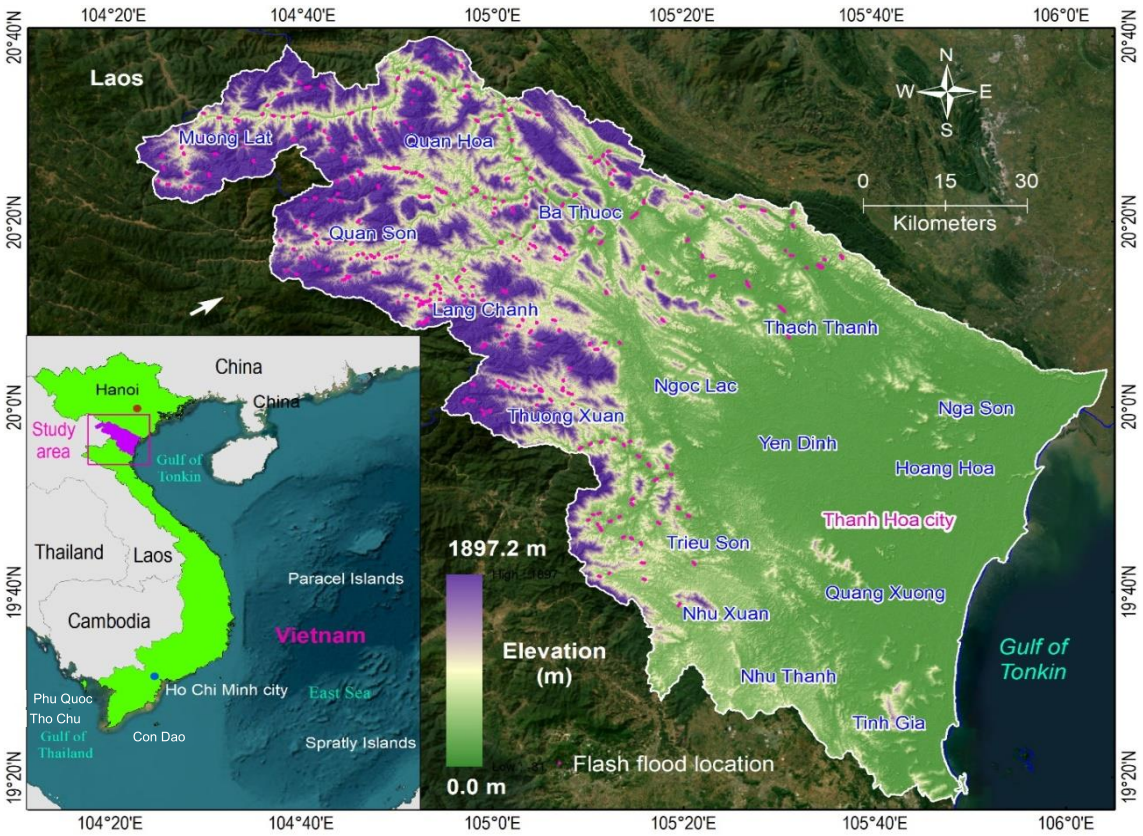

Figure 1. Geographic positioning of Thanh Hoa Province and the locations of flash-flood incidents

2.2. Data

2.2.1. Flash-flooded inventory

For this analysis, we relied on the flash-flood inventory map created in a previous investigation within the scope of research project VAST05.01/21-22, sponsored by the Vietnam Academy of Science and Technology (Hoa et al., 2024).

A total of 2,540 flash flood sites were mapped through change detection analysis (Psomiadis, 2016) of Sentinel-1 SAR imagery. Herein, flash floods resulting from tropical storms during the five-year period from 2018 to 2022, which caused substantial precipitation and ensuing flash floods, were utilized.

Initially, we compiled a list of tropical cyclones and storms affecting Thanh Hoa Province using reports from Vietnamese media, prioritizing heavy rains known to cause substantial flash floods and landslides. Significantly, the timeframe from July 7, 2021, to August 31, 2021, was identified as particularly important due to various flash flood events (Hoa et al., 2024). During this period, the study area was affected by a tropical depression emerging from the East Sea, resulting in intense downpours. The minimum and maximum recorded rainfalls were 1,069.9 mm and 1,023.9 mm, respectively.

Sentinel-1 images recorded before and after flash flood events were collected to detect the flash flood sites. These images underwent a comprehensive processing protocol to recognize and position flash flood occurrences (Trong et al., 2023). The process

began with image calibration, converting raw SAR pixel values to radar backscatter values that denote surface reflectivity. This was followed by speckle filtering to reduce the noise in SAR images.

Then, the georeferencing process was carried out to adjust the images to a specific coordinate system, ensuring accurate comparisons between the pre-and post-flood images. Subsequently, flash flood areas were manually identified and delineated. The initial flash flood map was refined using additional criteria such as slope, land cover, and hill shading to reduce false positives and improve accuracy. Finally, on-site surveys were carried out to validate the detected flood sites. This involved visiting the identified areas to confirm the presence and extent of flooding, thereby enhancing the reliability of the satellite-based flood detection.

2.2.2. Flash flood indicators

This study's approach to modeling flash floods hinges on correlating historical flash flood events with their influencing factors to predict future occurrences. Consequently, the precision of these predictions is highly dependent on the meticulous selection of these influencing factors. In a previous study, Hoa et al. (2024) evaluated the correlations between flash flooding and twelve flash flood indicators (soil type, geology, land use/land cover (LULC), stream density, Normalized Difference Vegetation Index (NDVI), Normalized Difference Water Index (NDWI), elevation, topographic wetness index (TWI), slope, aspect, curvature, and rainfall). Based on these findings, the current study employs these twelve indicators (Fig. 2) for flash flood modeling.

The soil type map (Fig. 2a) was generated from national pedology maps at a scale of 1:100,000, issued by the Ministry of Agriculture and Rural Development of Vietnam. For this analysis, the original 32 soil types from the pedology maps have been consolidated into 16 generalized categories for flash-flood modeling. The geological map (Fig. 2b) was derived from the Geological and Mineral Resources Maps at a scale of 1:200,000, issued by the Ministry of Natural Resources and Environment of Vietnam. Utilizing the material components and degree of weathering (Tien Bui et al., 2012), the map was compiled into 20 categories. The land use/land cover (LULC) map of Thanh Hoa Province with 10 categories (Fig. 2c) was developed using a 2020 LULC dataset provided by the Japan Aerospace Exploration Agency (JAXA) (www.eorc.jaxa.jp). The LULC has a resolution of 30 m.

Regarding the stream density, the stream density map (Fig. 2d) was computed based on the stream network derived from OpenStreetMap (www.openstreetmap.org; accessed on February 15, 2023). The stream density map was then produced via the Line Density tool in ArcGIS Pro. In Fig. 2d, the density map for Thanh Hoa Province reveals values ranging from 0.0 to 4.7 km/km².

NDVI and NDWI indices were chosen for this study's flash flood modeling due to their effectiveness in capturing essential surface data regarding vegetation vitality and moisture content (Hoa et al., 2024). Besides, Landsat 8 OLI imagery, with a 30-meter spatial resolution and accessed on February 15, 2023, from www.earthexplorer.usgs.gov, was employed in this study to create the NDVI map (Fig. 2e) and NDWI map (Fig. 2f) for Thanh Hoa Province. The NDVI map and the NDWI map were derived following the method outlined in Equation 1 (Defries and Townshend, 1994) for NDVI and Equation 2 (Xu, 2006) for NDWI, as detailed below:

$$NDVI = (Band\ 5 - Band\ 4)/(Band\ 5 + Band\ 4) \quad (1)$$

$$NDWI = (Band\ 5 - Band\ 6)/(Band\ 5 + Band\ 6) \quad (2)$$

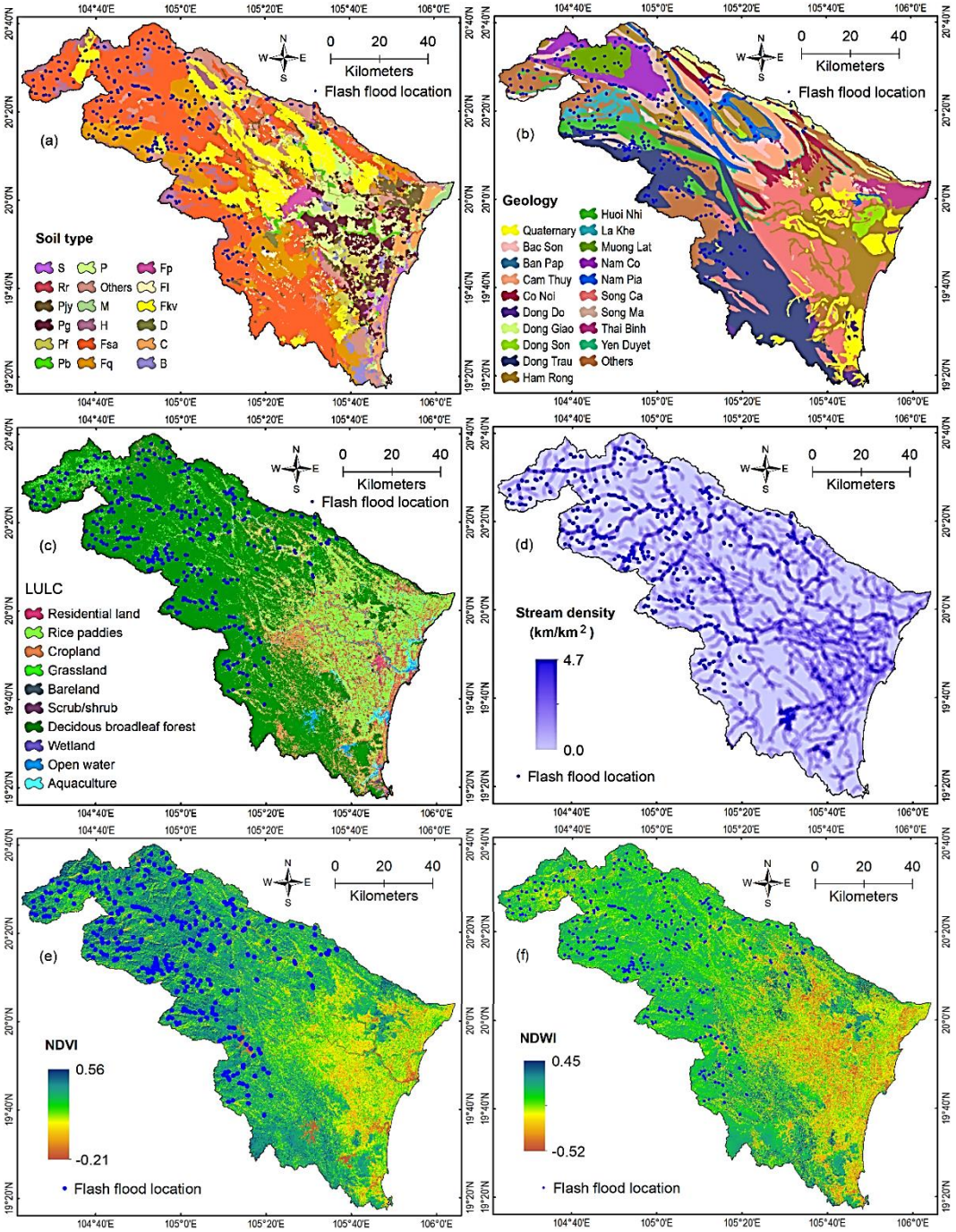

Figure 2. Flash-flood indicators: (a) Soil type; (b) Geology; (c) LULC; (d) Stream density; (e) NDVI; (f) NDWI; (g) Elevation; (h) TWI; (i) Slope; (j) Aspect; (k) Curvature; and (l) Rainfall. Abbreviation for Soil type: S: Neutral saline soil; Rr: Black soil on serpentine; Pjy: Alluvial soil in streams and waterlogged areas; Pg: Gley alluvial soil; Pf: Alluvial soil with mottled layers; Pb: Accumulated alluvial soil; P: Alluvial soil without recent deposition; Others: Other soils; M: Moderately saline soil; H: Humus soil; Fsa: Red-yellow soil; Fq: Light yellow soil on sandstone; Fp: Yellow-brown soil on ancient alluvium; Fkv: Red-brown soil; D: Colluvial valley soil; C: Coastal sandy soil; B: Degraded grey soil on ancient alluvium

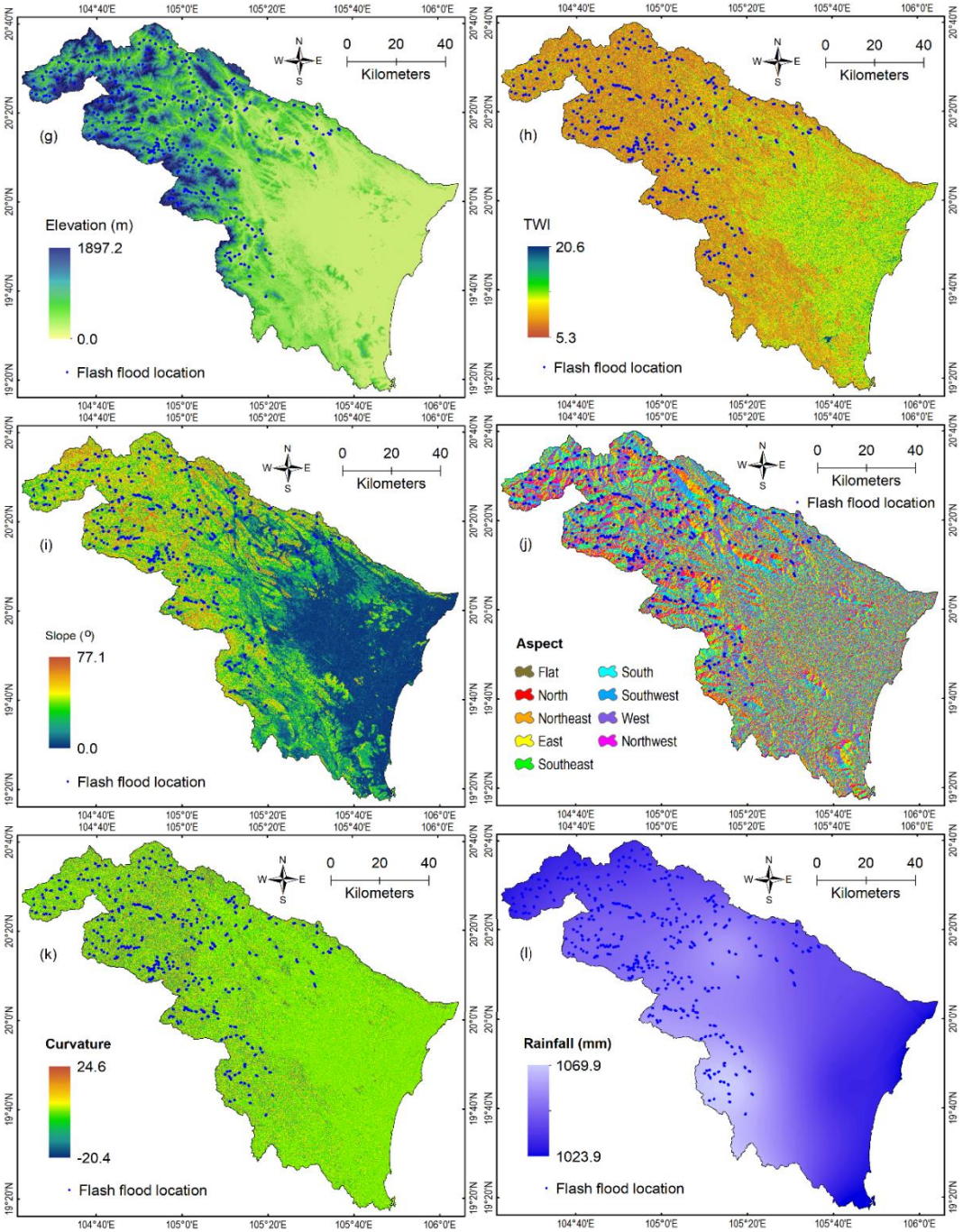

Figure 2. Cont.

In flash flood modeling, topography and terrain features significantly influence water flow during rainfall (Zevenbergen and Thorne, 1987). Consequently, these factors were incorporated into the modeling. For this study, the digital elevation model (DEM) of Thanh Hoa Province was obtained from the ALOS DEM, featuring a 30-meter resolution and supplied by JAXA, accessible at www.eorc.jaxa.jp (accessed on February 15,

2023). Employing this DEM, five morphometric factors were produced using the Spatial Analysis tool in ArcGIS Pro. These factors include elevation, TWI, slope, aspect, and curvature. Figure 2g shows the province's elevation map with elevation values ranging from 0.0 m to 1897.2 m. For the case of the TWI map (Fig. 2h), the TWI values span from 5.3 to 20.6. Within Thanh Hoa Province, the slope map's values vary from 0.0 to 77.1 degrees (Fig. 2i). The aspect map was compiled with nine slope directions (Fig. 2j). Lastly, for the curvature map (Fig. 2k), the curvature values range from -20.4 to 24.6.

Regarding rainfall, this factor is crucial in shaping and directing the water flow within a watershed, significantly influencing the magnitude, velocity, and behavior of flood flows (Bryndal et al., 2017). Determining the paths water takes as it travels over the terrain affects how quickly water accumulates and flows, impacting the intensity and speed of flash floods. Additionally, this factor dictates how water interacts with the landscape, influencing erosion, sediment transport, and the overall dynamics of floodwaters (Hamidifar et al., 2024), thereby playing a pivotal role in the hydrological response of a watershed during flash flood events. As detailed in Section 2.2, we analyzed the most critical rainfall incidents that resulted in flash floods in Thanh Hoa Province during the five years from 2018 to 2022. The timeframe from July 7, 2021, to August 31, 2021, stands out for its connection to a serie of flash flood events. Consequently, the total rainfall during this period was used to create the map (Figure 2l) applying the Inverse Distance Weighting (IDW) interpolation technique in ArcGIS Pro. The rainfall data was drawn from the climate resources provided by the NASA POWER project.

3. Background of the algorithms used

3.1. Random Forest

As formulated by Breiman (2001), Random Forest serves as a robust and extensively utilized ensemble learning approach for tasks in classification and regression. In flash flood modeling, the Random Forest algorithm can effectively handle the complexities and nonlinearities inherent in environmental data (Tan et al., 2024), providing reliable predictions based on a combination of multiple decision trees.

Consider a dataset for flash floods, referred to as FFD, which contains n samples organized as FFD $\in$ (X,y). In the context of this analysis, X is structured as a matrix with m rows and 12 columns, with each column indicating a distinct flash flood indicator. The matrix y, with m rows and a single column, specifies the presence (which is coded as 1) or absence (which is coded as 0) of historical flash floods at various locations. The aim is to develop a predictive model, FF(X)→[0,1], by employing the random forest algorithm. Employing the FFD, the random forest algorithm produces L subsets using bootstrap aggregating, often called "bagging". Subsequently, each of these subsets is utilized to create each decision tree separately. The individual decision trees are then combined to produce an ensemble model. Finally, the voting mechanism of the classification task is used where each tree votes for a class, and the final prediction is the majority vote, where the probability values for the presence class are used for flash flood indices.

The effectiveness of the random forest (RF) model is significantly influenced by the forest's tree count (TotalTree), the maximum depth limit for each tree (MaxTree), and the number of flood indicators incorporated (nfloodTree). Therefore, the careful selection of these parameters is essential. To address this, the study introduces a new approach that

employs BCMO to search for and optimize these parameters effectively. The details of this optimization method are presented in the following section.

3.2. Balancing Composite Motion Optimization

Balancing Composite Motion Optimization (BCMO), is a high-level population-based optimization algorithm, initially introduced by Le-Duc et al. (2020). It is designed to efficiently search for and optimize multiple parameters within complex models. BCMO combines principles from several optimization techniques to balance exploration and exploitation, facilitating an extensive search across the solution space while converging on optimal or near-optimal solutions. BCMO offers a powerful and flexible approach for optimizing the parameters of the RF model. Its ability to balance exploration and exploitation, combined with a composite motion strategy, allows for effective navigation of complex solution spaces and enhances model performance (Tuan et al., 2023). The key features of BCMO for optimizing the random forest model in flash flood modeling in this research are as follows:

(1) Population Initialization

After defining the search space, population, and objective function, BCMO sets up a population of solution candidates at the outset. Each candidate represents a possible set of parameters for the random forest model, including TotalTree, MaxTree, and nfloodTree. The initial distribution and placement of the candidate solutions are determined using Eq.3.

$$POS_i = LB_i + \text{rand}\,(1, S) \times (UB_i - LB_i) \quad (3)$$

where POS_i, UB_i, and LB_i are defined by the position, maximum constraint, and minimum constraint of the candidate solution. The parameter S denotes the dimension of the search space.

Subsequently, each candidate solution is evaluated for fitness based on the established objective function and ranked to identify the optimal individual.

(2) Composite Motion Strategy and Balancing Mechanism

The algorithm employs a composite motion strategy, combining various movement patterns, taking cues from natural processes and other related optimization techniques. This strategy ensures that the search process is diversified, preventing premature convergence on local optima (Le-Duc et al., 2020). A balancing mechanism is incorporated to fine-tune the balance between dynamic exploration (discovering new regions in the solution space) and exploitation (enhancing existing optimal solutions). This mechanism preserves population diversity and improves the algorithm's capacity to identify high-quality solutions. Thus, in each iteration (it), the position of the i^{th} candidate solution is revised according to Eq. 4, shown below.

$$POS_i^{it+1} = POS_i^{it} + v_{i/j} + v_j \quad (4)$$

where $\mathbf{v_{i/j}}$ presents the relative displacement of the i^{th} candidate solution concerning the j^{th} candidate, and v_j denotes the directional vector of the j^{th} candidate.

(3) Fitness Evaluation, Selection, and Update

Each candidate solution's fitness is assessed according to its effectiveness in the random forest model using the objective function. The selection process, guided by fitness evaluations, identifies which candidates to preserve and which to substitute. Then, the positions of the selected candidates are updated according to the composite motion strategy (Equation 4 above).

(4) Termination Criteria

Steps 2 and 3 are repeated until a set termination condition is satisfied, resulting in the identification of the best candidate solution.

3.2. Proposed approach using Balancing Composite Motion Optimized Random Forest for Spatial Prediction of Flash Flood

The flowchart of the proposed approach, which integrates BCMO and RF for mapping flash flood modeling, is illustrated in Fig. 3.

The Matlab code for the BCMO algorithm is available in Le-Duc et al. (2020), whereas the authors developed the BCMO-RF model in the Matlab environment.

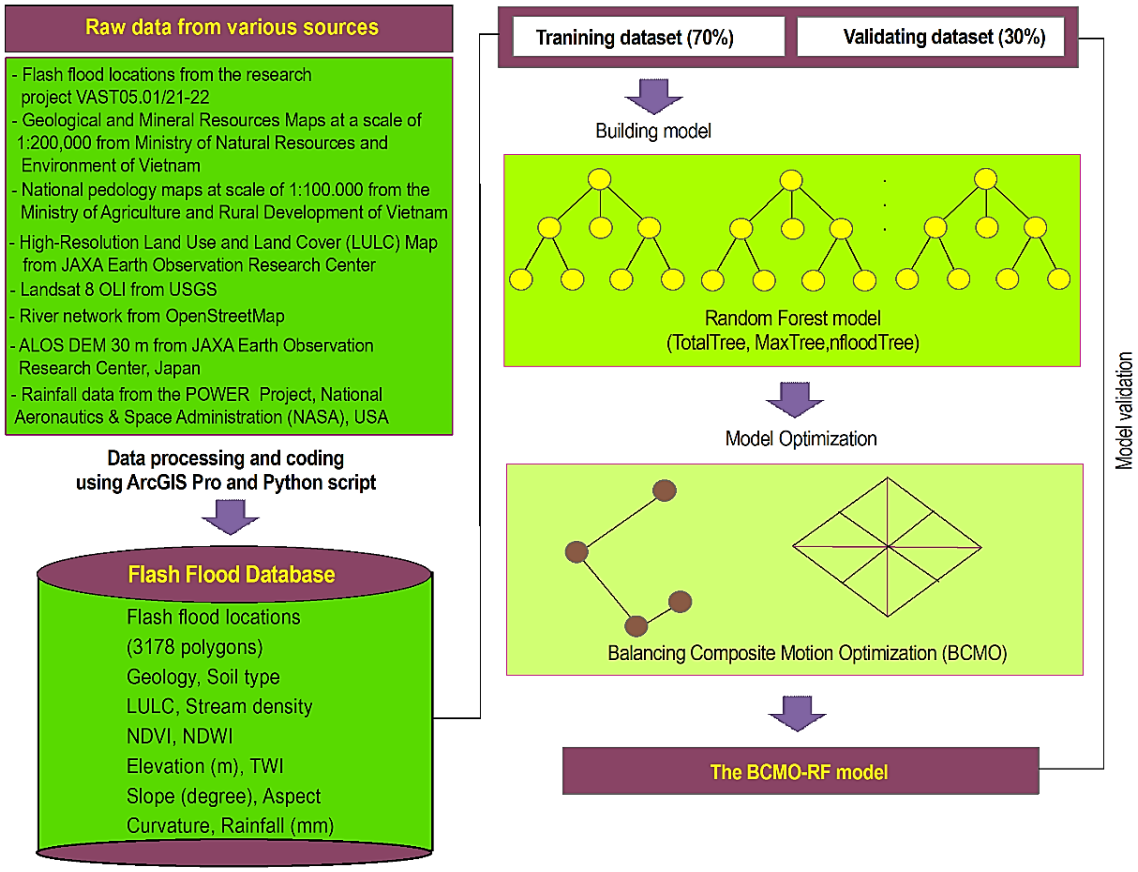

Figure 3. The flowchart illustrates the proposed approach

3.2.1. Flash flood database

In the previous work (Hoa et al., 2024), the flash flood database was constructed using the 2540 flash flood sites and 12 flash flood indicators. The coordinate system of the database was set to WGS 1984 UTM Zone 48N. All indicators were standardized to a raster format at 30 m resolution and normalized between 0.01–0.99.

In addition to the 2,540 flash flood sites, a proportional number of points representing non-flood sites were also sampled, resulting in 5,080 samples for flash flood modeling. Locations with flash floods were labeled "1," and those without were labeled "0.". Using ArcGIS Pro's sample tool, a sampling operation was subsequently executed to gather values for ten influencing factors at these locations. Next, the dataset was randomly partitioned, with 70% allocated to the training set and 30% to the validation set, consisting of 3,556 and 1,524 samples, respectively.

3.2.2. Objective function

As described in Section 3.2, the Random Forest algorithm was used to build the flash flood model, with BCMO applied to search for and optimize three model parameters: TotalTree, MaxTree, and nfloodTree. In this context, the 3D coordinates of the candidate solution correspond to these three parameters. Throughout the training phase, the parameters

of the BCMO-RF model were examined and adjusted within the search space to identify the optimal Random Forest model. The fitness of these parameters was assessed with the Mean Squared Error (MSE) serving as the objective function (Tuan et al., 2023), as below:

$$\text{MSE} = \frac{1}{n}\sum_{i=1}^{n}(FL_i - FLO_i)^2 \qquad (5)$$

where FFL_{i} signifies the flash flood value sourced from the inventory map, while FLO_i Represents the flash flood estimation generated by the proposed BCMO-RF model; n denotes the total number of samples used in the analysis.

3.2.3. Model Setup

Configuring the RF model requires specifying three parameters: TotalTree, MaxTree, and nfloodTree. Consequently, a 3-dimensional search space (S) was established. These parameters were organized into a 1×S matrix. The maximum constraint (LB) and minimum constraint (UB) (Eq.3) were set to -1 and 1, respectively. A population of 85 candidate solutions was chosen, with a maximum of 2,000 iterations (Tuan et al., 2023). Within the search space S, the coordinates of each candidate solution in the 3-dimensional space were obtained, making each position a potential solution for the BCMO-RF model. As individuals move to new positions, new solutions are generated and tested. The optimization process aims to discover the position where MSE is at its minimum.

3.3.4. Performance assessment

To evaluate how well the proposed BCMO-RF model performs in predicting flash flood occurrences spatially, we employed the following statistical metrics: True Positive (TP), False Positive (FP), False Negative (FN), and True Negative (TN) rates (Degiorgis et al., 2013). By leveraging these metrics, the following performance indicators were derived: Positive Predictive Value (PPV) (Eq. 6), which measures the proportion of accurate flash flood predictions; Negative Predictive Value (NPV) (Eq. 7), which indicates the proportion of accurate non-flash flood predictions; Sensitivity (Sens) (Eq. 8), also known as recall, which assesses the model's competence in accurately predict flash flood locations; and Specificity (Spec) (Eq. 9), which measures the model's capacity to predict non-flood locations accurately. Accuracy (Eq.10) demonstrates the model's overall accuracy in predicting both flood and non-flood locations.

$$\text{PPV}=\text{TP}/(\text{TP}+\text{FP}) \qquad (6)$$

$$\text{NPV}=\text{TN}/(\text{TN}+\text{FN}) \qquad (7)$$

$$\text{Sensitivity}=\text{TP}/(\text{TP}+\text{FN}) \qquad (8)$$

$$\text{Specificity}=\text{TN}/(\text{FP}+\text{TN}) \qquad (9)$$

$$\text{Accuracy}=(\text{TP}+\text{TN})/(\text{TP}+\text{FP}+\text{FN}+\text{TN}) \qquad (10)$$

In addition, the Receiver Operating Characteristic (ROC) Curve (Pepe, 2000), which plots the true positive rate (Sensitivity) versus the false positive rate (1 - Specificity) at multiple threshold levels, was also used. The Area Under the ROC Curve (AUC) was used to measure the overall performance of the BCMO-RF model.

3.2.5. Reference Model and Creation of the Flash Flood Susceptibility Map

In this study, the effectiveness of the proposed BCMO-RF model is showcased via a comparative analysis with the prior established Deep 1D-CNN model (Hoa et al., 2024) for flash flood prediction. Successful training and validation of the BCMO-RF model facilitated the computation of flash flood susceptibility indices throughout the study area, which were converted into GIS format, resulting in the construction of the final susceptibility map.

4. Results and analysis

4.1. Model training and validating

During the training phase, the BCMO-RF model was developed using the training dataset, where the three parameters, TotalTree, MaxTree, and nfloodTree, are searched and optimized through 2000 iterations. The best values found are: TotalTree is 212, MaxTree is 15, and nfloodTree is 4. To mitigate the risk of overfitting, a 10-fold cross-validation technique was utilized during the training phase of the BCMO-RF model. The result is shown in Table 1 and Fig. 4. The results indicate that the BCMO-RF model performs robustly in classifying flash flood events. Specifically, the PPV is 92.7%, signifying that the model accurately identifies flash flood pixels in 95.59% of instances. The NPV stands at 93.8%, which means the model correctly classifies pixels as non-flash floods with a 93.8% accuracy.

Table 1. Performance of the BCMO-RF model in the training phase (using the 10-fold cross-validation technique) and the validation phase

Flash Flood model	Statistical metrics										
	TP	TN	FP	FN	PPV (%)	NPV (%)	Sens (%)	Spec(%)	Acc	Kappa	AUC
Training phase											
BCMO-RF	1649	1667	129	111	92.7	93.8	93.7	92.8	93.3	0.865	0.981
1D-CNN	1650	1603	128	175	92.8	90.2	90.4	92.6	91.5	0.830	0.977
Validating											
BCMO-RF	712	716	50	46	93.4	94.0	93.9	93.5	93.7	0.874	0.988
1D-CNN	694	681	68	81	91.1	89.4	89.5	90.9	90.2	0.804	0.969

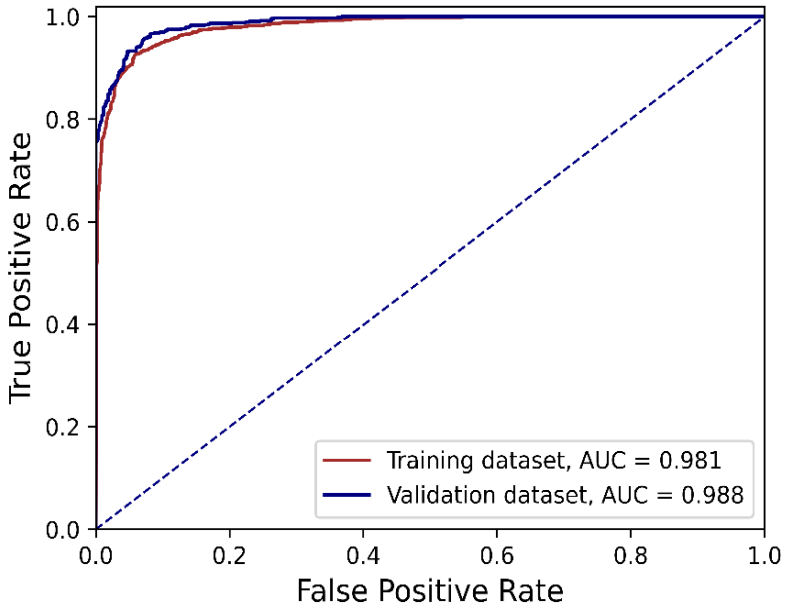

Figure 4. ROC curve and AUC of the BCMO-RF model in the training phase and the validation phase

Additionally, the model's Sens is 93.7%, demonstrating its efficacy in correctly identifying locations of flash floods. Spec is 92.8%, reflecting the model's competence to identify non-flood locations accurately. The model's overall accuracy (Acc) is 93.3%,

indicating its general effectiveness in predicting flood and non-flood locations. Furthermore, the Kappa statistic is 0.865, suggesting that the BCMO-RF model's performance is 86.5% better than a random classification, underscoring its reliability and precision in flash flood prediction tasks. The AUC is 0.981, signifying that the model's overall performance is excellent, with a global performance rate of 98.1%.

By using the validation set, the prediction capability of the proposed BCMO-RF model is verified, and the result is also shown in Table 1 and Fig. 4. The evaluation metrics indicate that the BCMO-RF model demonstrates high prediction performance in classifying flash flood locations. The PPV is 93.4%, which signifies that when the model predicts a flash flood, it is correct in 93.4% of the cases. The NPV is 94.0%, showing that the model correctly identifies non-flash flood pixels with 94.0% accuracy. The model's sensitivity is 93.9%, indicating its effectiveness in detecting flash flood locations. The specificity is 93.5%, reflecting its ability to predict non-flood locations accurately. The overall prediction accuracy of the model is 93.7%, demonstrating its general reliability in predicting flood and non-flood areas. Moreover, the Kappa statistic is 0.874, which means the model's performance is 87.4% better than random chance. The AUC is 0.988, signifying that the prediction performance of the model is excellent, with a global performance rate of 98.1%

4.2. Comparative Assessment and Statistical Examination

To assess the capabilities of the proposed BCMO-RF model, we conducted a comparative analysis against the established benchmark, the Deep 1D-convolution neural network (Deep 1D-CNN) model, as demonstrated in prior research. The detailed design and explanation of the Deep 1D-CNN model are presented by Hoa et al. (2024). This comparison aimed to evaluate both models' performance and predictive capabilities. The result is shown in Table 1 and Fig. 4.

It could be seen that, during the training phase, using the 10-fold cross-validation technique, the BCMO-RF model demonstrated superior performance across several statistical metrics compared to the 1D-CNN model. The BCMO-RF model achieved a PPV of 92.7% and a Negative Predictive Value (NPV) of 93.8%, while the 1D-CNN model recorded an almost equal PPV of 92.8% but a lower NPV of 90.2%. The sensitivity (Sens) of the BCMO-RF model was 93.7%, indicating a higher ability to correctly identify flash flood locations compared to the 1D-CNN model's 90.4%. The specificity (Spec) of the BCMO-RF model was almost equal at 92.8% compared to 92.6% for the Deep 1D-CNN. In terms of overall accuracy (Acc), the BCMO-RF model achieved 93.3%, outperforming the Deep 1D-CNN model's accuracy of 91.5%. The Kappa statistic, which measures the agreement between observed and predicted classifications, was higher for the BCMO-RF model (0.865) compared to the Deep 1D-CNN model (0.830). Finally, the Area Under the Curve (AUC) was 0.981 for the BCMO-RF model, indicating excellent global performance, slightly better than the Deep 1D-CNN model's AUC of 0.977.

The result in the validation phase indicated that the BCMO-RF model outperformed the Deep 1D-CNN model across most metrics. The BCMO-RF model achieved a PPV of 93.4% and an NPV of 94.0%, whereas the

Deep 1D-CNN model recorded lower values of 91.1% and 89.4%, respectively. The sensitivity of the BCMO-RF model was 93.9%, surpassing the Deep 1D-CNN model's 89.5%, and its specificity was 93.5% compared to the Deep 1D-CNN's 90.9%. The overall accuracy of the BCMO-RF model during the validation phase was 93.7%, significantly higher than the Deep 1D-CNN model's 90.2%. The Kappa statistic for the BCMO-RF model was 0.874, indicating a higher agreement rate compared to the Deep1D-CNN model's 0.804. Additionally, the BCMO-RF model achieved an AUC of 0.988, showcasing slightly better global performance over the Deep 1D-CNN model's AUC of 0.969. In summary, the BCMO-RF model demonstrated consistent and superior performance over the Deep 1D-CNN model in the training and validation phases, making it a more reliable choice for flash flood prediction in the study area.

A paired samples t-test was carried out to statistically verify whether the BCMO-RF model outperforms the Deep 1D-CNN model for flash flood prediction. The null hypothesis (H0) asserts that there is no significant difference in the predictive abilities of the two models within a 95% confidence interval for the difference in means. T-value and p-value were computed for the model pair. Rejection of the null hypothesis occurs if the t-value exceeds the range of -1.96 to +1.96 and the p-value is equal to or less than 0.05. The results presented in Table 2 show a t-value of 2.694, which lies outside the range of -1.96 to +1.96, along with a p-value of 0.007, which is below the significance level of 0.05. These findings demonstrate that the BCMO-RF model's predictive performance significantly exceeds that of the Deep 1D-CNN model.

Table 2. Paired samples t-test Analysis of the BCMO-RF model and the Deep 1D-CNN model for Spatial Flash Flood Prediction in this research

No.	Pairwise model	*t*-value	*p*-value	Significance
1	BCMO-RF model vs. Deep 1D-CNN	2.694	0.007	Yes

4.3. Flash-flood susceptibility map

To generate the flash flood susceptibility map, Thanh Hoa Province was organized into a matrix of 5,926 columns by 5,093 rows, corresponding to 30,181,118 pixels. The susceptibility index values for these pixels were then computed using the BCMO-RF model. The results indicate that the index values ranged from 0.000 to 1.000, representing varying degrees of flash flood susceptibility across the region. Then, the susceptibility map was projected into the WGS 1984 UTM Zone 48N coordinate system. This conversion facilitated the creation of a comprehensive flash flood susceptibility map, depicted in Fig. 5. The resulting map provides a detailed spatial representation of flash flood risks, enabling better planning and mitigation strategies in the study area.

Examination of the susceptibility map highlights a notable flash flood risk in specific districts, among them Muong Lat, Ba Thuoc, and Trieu Son (Fig. 5). These regions consistently have experienced severe flash floods in the last three years. The primary contributing factors are the elevated altitudes and steep slopes of the terrain, which exacerbate water runoff and increase the speed and intensity of flash floods. These geographical characteristics make these districts particularly vulnerable during heavy rainfall events. Conversely, southeastern districts like Hoang Hoa, Nga Son, Quang Xuong, and Hoang Hoa demonstrate a markedly lower risk of flash floods.

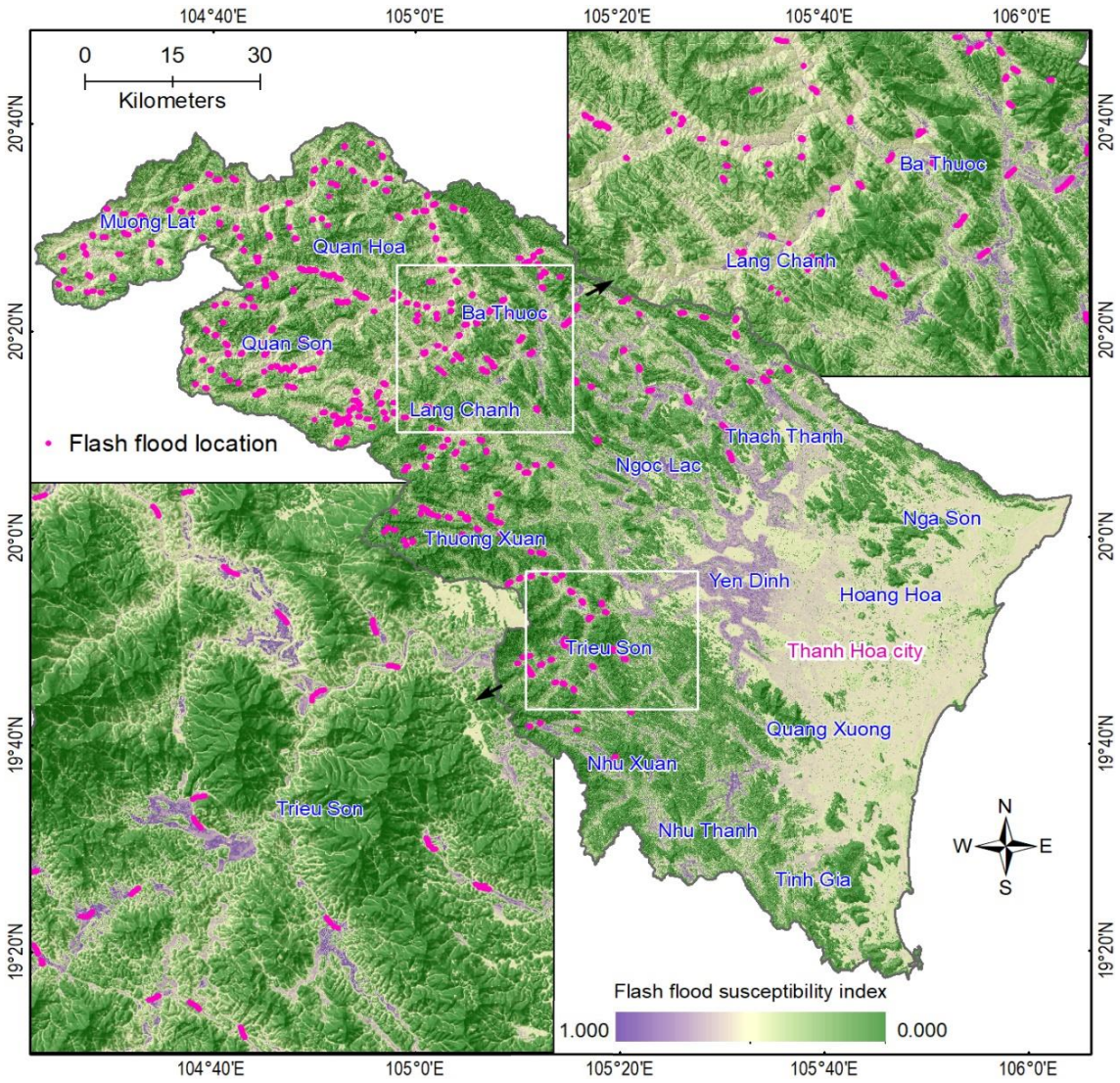

Figure 5. Flash flood susceptibility map for the study area using the BCMO-RF model

5. Discussions

While forecasting flash floods is still a significant challenge (Ding et al., 2021; Saint-Fleur et al., 2023), assessing and identifying vulnerable areas beforehand can be a proactive approach to mitigate the risks associated with flash floods (Pham et al., 2020). This study proposes and validates a significant advancement in methodology that enhances the predictive accuracy of flash floods. Specifically, the RF model is utilized to establish flood prediction models, while the BCMO technique is employed to fine-tune three key parameters: TotalTree, MaxTree, and nfloodTree.

The introduction and successful application of the BCMO-RF model represent a significant improvement in prediction accuracy compared to the state-of-the-art Deep 1D-CNN (Hoa et al., 2024). The statistical test results demonstrate that the BCMO-RF model significantly surpasses the benchmark. This denotes a statistically

significant improvement in predictive performance, which is essential for areas susceptible to frequent and severe rainfall, such as this study area. Herein, the BCMO-RF model outperforms the Deep 1D-CNN in its ensemble learning framework in flash flood prediction, which assembles multiple decision trees to enhance prediction precision and reduce overfitting.

One of the standout features of the BCMO-RF model is its robustness and adaptability to different environmental conditions. By incorporating BCMO, the model can manage the variability in the geo-environmental patterns of the study area. This adaptability is crucial for maintaining the model's effectiveness under diverse and changing climatic conditions. The ability of the BCMO-RF model to accurately predict flash floods stems from its sophisticated algorithm, which effectively balances composite motion and optimizes the random forest approach. This ensures the model can handle the complex interplay of various meteorological and geographical factors influencing flash floods.

Despite its success, the BCMO-RF model does face particular challenges and limitations. The complexity of the model requires significant computational resources and technical expertise to implement and maintain effectively. Additionally, the model's performance is highly dependent on the quality and granularity of the input data. In this research, these data were collected and processed from multiple sources with different resolutions and scales; therefore, it is challenging to eliminate uncertainties.

In addition, while the model has shown promising results for Thanh Hoa province, its effectiveness in other regions with different climatic and topographical conditions must be validated through further research. Addressing the identified limitations and expanding the applicability of the BCMO-RF model are crucial for future research. One important direction is to consider the model in diverse geographical regions, i.e., the mountain areas of northern Vietnam, to understand its versatility and limitations. This would involve testing the model in areas with different climatic patterns, topographies, and urbanization levels.

6. Conclusions

In conclusion, the proposed BCMO-RF model exhibits high accuracy and reliability, with enhanced performance metrics that validate its effectiveness in predicting flash flood occurrences. The improved robustness and adaptability of the BCMO-RF model make it a valuable tool for disaster management and mitigation efforts. However, addressing the model's limitations and pursuing further research opportunities is essential to fully realize its potential and broaden its applicability across different regions.

Future work could focus on refining the model by integrating additional environmental variables, exploring the use of real-time data for dynamic prediction, and testing the model in diverse geographical settings to assess its generalizability. Additionally, incorporating community-based data and local knowledge could enhance the model's accuracy and relevance in specific contexts. This study underscores the importance of continued innovation in predictive modeling to better prepare for and mitigate the impacts of flash flood hazards.

Funding

This research was funded by the Vietnam Academy of Science and Technology (VAST), Vietnam. The grant number is VAST05.01/21-22.

Data Availability Statement

The data presented in this study are available on request from the first author. The data are not publicly available due to privacy.

Conflicts of Interest

The authors declare no conflict of interest.

References

Abedi R., Costache R., Shafizadeh-Moghadam H., Pham Q.B., 2022. Flash-flood susceptibility mapping based on XGBoost, random forest and boosted regression trees. Geocarto International, 37(19), 5479–5496.

Amiri A., Soltani K., Ebtehaj I., Bonakdari H., 2024. A Novel Machine Learning Tool for Current and Future Flood Susceptibility Mapping by Integrating Remote Sensing and Geographic Information Systems. Journal of Hydrology, 130936.

Bournas A., Baltas E., 2022. Investigation of the gridded flash flood Guidance in a Peri-Urban basin in greater Athens area, Greece. Journal of Hydrology, 610, 127820.

Breiman L., 2001. Random forests. Machine learning, 45, 5–32.

Bryndal T., Franczak P., Kroczak R., Cabaj W., Kołodziej A., 2017. The impact of extreme rainfall and flash floods on the flood risk management process and geomorphological changes in small Carpathian catchments: a case study of the Kasiniczanka river (Outer Carpathians, Poland). Natural Hazards, 88(1), 95–120.

Bui D.T., Ngo P.-T.T., Pham T.D., Jaafari A., Minh N.Q., Hoa P.V., Samui P., 2019. A novel hybrid approach based on a swarm intelligence optimized extreme learning machine for flash flood susceptibility mapping. Catena, 179, 184–196.

Degiorgis M., Gnecco G., Gorni S., Roth G., Sanguineti M., Taramasso, A.C., 2013. Flood hazard assessment via threshold binary classifiers: case study of the Tanaro river basin. Irrigation and Drainage, 62(S2), 1–10.

Ding L., Ma L., Li L., Liu C., Li N., Yang Z., Yao Y., Lu H., 2021. A survey of remote sensing and geographic information system applications for flash floods. Remote Sensing, 13(9), 1818.

Dinh T.N., Thi H.L., 2024. Models of residential space for ethnic minorities in Thanh Hoa Province associated with sustainable livelihoods. Heritage and Sustainable Development, 6(1), 127–144.

Godara N., Bruland O., Alfredsen K., 2023. Simulation of flash flood peaks in a small and steep catchment using rain-on-grid technique. Journal of Flood Risk Management, 16(3), e12898.

Group W.B., Bank A.D., 2021. Climate Risk Country Profile: Vietnam. World Bank.

Guo K., Guan M., Yu D., 2021. Urban surface water flood modelling a comprehensive review of current models and future challenges. Hydrology and Earth System Sciences, 25(5), 2843–2860.

Hamidifar H., Nones M., Rowinski P.M., 2024. Flood modeling and fluvial dynamics: A scoping review on the role of sediment transport. Earth-Science Reviews, 253, 104775.

Hoa P.V., Binh N.A., Hong P.V., An N.N., Thao G.T.P., Hanh N.C., Ngo P.T.T., Bui D.T., 2024. One-dimensional deep learning driven geospatial analysis for flash flood susceptibility mapping: A case study in North Central Vietnam. Earth Science Informatics, 1–22.

Jodar-Abellan A., Valdes-Abellan J., Pla C., Gomariz-Castillo F., 2019. Impact of land use changes on flash flood prediction using a sub-daily SWAT model in five Mediterranean ungauged watersheds (SE Spain). Science of the Total Environment, 657, 1578–1591.

Knocke E.T., Kolivras K.N., 2007. Flash flood awareness in southwest Virginia. Risk Analysis: An International Journal, 27(1), 155–169.

Le-Duc T., Nguyen Q.-H., Nguyen-Xuan H., 2020. Balancing composite motion optimization. Information Sciences, 520, 250–270.

Linh L.K., Vinh L.Q., Truong N.Q., 2019. New records of skinks (Squamata: Scincidae) from Nam Dong valuable Gymnosperm conservation area, Thanh Hoa province. Journal of Forestry Science and Technology, 8, 109–116.

Ngo P.-T.T., Pham T.D., Hoang N.-D., Tran D.A., Amiri M., Le T.T., Hoa P.V., Van Bui P., Nhu V.-H., Bui D.T., 2021. A new hybrid equilibrium optimized SysFor based geospatial data mining for tropical storm-induced flash flood susceptible mapping. Journal of Environmental Management, 280, 111858.

Pepe, M.S., 2000. Receiver operating characteristic methodology. Journal of the American Statistical Association, 95(449), 308–311.

Pham N.T.T., Nong D., Sathyan A.R., Garschagen M., 2020. Vulnerability assessment of households to flash floods and landslides in the poor upland regions of Vietnam. Climate Risk Management, 28, 100215.

Plate E.J., 2007. Early warning and flood forecasting for large rivers with the lower Mekong as example. Journal of Hydro-environment Research, 1(2), 80–94.

Psomiadis E., 2016. Flash flood area mapping utilising SENTINEL-1 radar data, Earth resources and environmental remote sensing/GIS applications VII. SPIE, 382–392.

Sabău D.A., Şerban G., Breţcan P., Dunea D., Petrea D., Rus I., Tanislav D., 2023. Combining radar quantitative precipitation estimates (QPEs) with distributed hydrological model for controlling transit of flash-flood upstream of crowded human habitats in Romania. Natural Hazards, 116(1), 1209–1238.

Saint-Fleur B.E., Allier S., Lassara E., Rivet A., Artigue G., Pistre S., Johannet A., 2023. Towards a better consideration of rainfall and hydrological spatial features by a deep neural network model to improve flash floods forecasting: case study on the Gardon basin, France. Modeling Earth Systems and Environment, 9(3), 3693–3708.

Suresh S., Hossain F., Minocha S., Das P., Khan S., Lee H., Andreadis K., Oddo P., 2024. Satellite-based tracking of reservoir operations for flood management during the 2018 extreme weather event in Kerala, India. Remote Sensing of Environment, 307, 114149.

Tan X., Li Y., Wu X., Dai C., Zhang X., Cai Y., 2024. Identification of the key driving factors of flash flood based on different feature selection techniques coupled with random forest method. Journal of Hydrology: Regional Studies, 51, 101624.

Tien Bui D., Pradhan B., Lofman O., Revhaug I., Dick O.B., 2012. Landslide susceptibility mapping at Hoa Binh province (Vietnam) using an adaptive neuro-fuzzy inference system and GIS. Computers & Geosciences, 45, 199–211.

Trong N.G., Quang P.N., Cuong N.V., Le H.A., Nguyen H.L., Tien Bui D., 2023. Spatial Prediction of Fluvial Flood in High-Frequency Tropical Cyclone Area Using TensorFlow 1D-Convolution Neural Networks and Geospatial Data. Remote Sensing, 15(22), 5429.

Tsangaratos P., Ilia I., Chrysafi A.-A., Matiatos I., Chen, W., Hong H., 2023. Applying a 1D Convolutional Neural Network in Flood Susceptibility Assessments: The Case of the Island of Euboea, Greece. Remote Sensing, 15(14), 3471.

Tuan T.A., Pha P.D., Tam T.T., Bui D.T., 2023. A new approach based on Balancing Composite Motion Optimization and Deep Neural Networks for spatial prediction of landslides at tropical cyclone areas. IEEE Access.

Tuyet Hanh T.T., Huong L.T.T., Huong N.T.L., Linh T.N.Q., Quyen N.H., Nhung N.T.T., Ebi K., Cuong N.D., Van Nhu H., Kien T.M., 2020. Vietnam climate change and health vulnerability and adaptation assessment, 2018. Environmental Health Insights, 14. https://doi.org/10.1177/1178630220924658.

Wang Y., Fu Z., Cheng Z., Xiang Y., Chen J., Zhang P., Yang X., 2024. Uncertainty analysis of dam-break flood risk consequences under the influence of non-structural measures. International Journal of Disaster Risk Reduction, 102, 104265.

Wdowinski S., Bray R., Kirtman B.P., Wu Z., 2016. Increasing flooding hazard in coastal communities due to rising sea level: Case study of Miami Beach, Florida. Ocean & Coastal Management, 126, 1–8.

Willner S.N., Levermann A., Zhao F., Frieler K., 2018. Adaptation required to preserve future high-end river flood risk at present levels. Science Advances, 4(1), eaao1914.

Zevenbergen L.W., Thorne C.R., 1987. Quantitative analysis of land surface topography. Earth Surface Processes and Landforms, 12(1), 47–56.

Zhao G., Liu R., Yang M., Tu T., Ma M., Hong Y., Wang X., 2022. Large-scale flash flood warning in China using deep learning. Journal of Hydrology, 604, 127222.